Proceedings of the VIII International Conference ION 2010, Kazimierz Dolny, Poland, June 14–17, 2010

Multilayered Nano–Microcomposite Ti–Al–N/TiN/Al_2O_3 Coatings. Their Structure and Properties

A.D. Pogrebnjak[a,*], A.P. Shpak[b], G.V. Kirik[c], N.K. Erdybaeva[d], M.V. Il'yashenko[a], A.A. Dem'yanenko[a], Yu.A. Kunitskii[b], A. Sh. Kaverina[a], V.S. Baidak[a], N.A. Makhmudov[e], P.V. Zukowski[f], F.F. Komarov[g], V.M. Beresnev[h], Sh.M. Ruzimov[e] and A.P. Shypylenko[a]

[a]Sumy Institute for Surface Modification, Sumy State University, St. 2 R-Korsakov, 40007 Sumy, Ukraine

[b]Institute of Metal Physics NAS of Ukraine, Kiev, Ukraine

[c]Concern "Ukrrosmetal", Sumy, Ukraine

[d]East-Kazakhstan State Technical University, Ust-Kamenogorsk, Kazakhstan

[e]Institute for Nuclear Physics, Ulugbek, Tashkent, Uzbekistan

[f]Lublin University of Technology, Lublin, Poland

[g]Belarus State University, Minsk, Belarus

[h]Kharkov National University, Kharkov, Ukraine

This paper presents the first results on formation and study of structure and properties of micro- and nanocomposite combined coatings. By means of modeling the deposition processes (deposition conditions, current density-discharge, plasma composition and density, voltage) we formed the three-layer nanocomposite coatings of Ti–Al–N/Ti–N/Al_2O_3. The coating composition, structure and properties were studied using physical and nuclear-physical methods. The Rutherford proton and helium ion backscattering, scanning electron microscopy with microanalysis, grazing incidence X-ray diffraction, as well as nanohardness tests (hardness) were used. Measurements of wear resistance and corrosion resistance in NaCl, HCl and H_2SO_4 solutions were also performed. For testing mechanical properties such characteristics of layered structures as hardness H, elastic modulus E: H^3/E^2 etc. were measured. It is demonstrated that the formed three-layer nanocomposite coatings have hardness of 32 to 36 GPa and elastic modulus of 328 ± 18 to 364 ± 14 GPa. Its wear resistance (cylinder-surface friction) increased by factor of 17 to 25 in comparison with the substrate (stainless steel). The layers thickness was in the range of 56–120 μm.

PACS: 61.46.–w, 62.20.Qp, 62.25.–q

1. Introduction

Traditional methods of surface modification (which are: physical, chemical, electrochemical and mechanical ones [1]) as well as more advanced methods such as ion implantation, ion-assisted deposition of thin films, plasma technologies and electron beam treatment [1–4] in some cases cannot result directly in a desirable way. In this connection for solving the industrial problems existing in ship building and chemistry, for instance [1, 5, 6], one has to combine such methods of surface modification for the production of hybrid coatings possessing the definite operation properties [1, 7]. An oxide-aluminum ceramics and other coatings based on titanium carbide and tungsten carbide and nitrides [1, 8–10] possess a number of useful properties, which are able to provide corrosion protection, high hardness and mechanical strength, low wear, and good electro-isolation properties.

It is well known that Ti–Al–N nanocomposite coatings feature high physical and mechanical properties such as high hardness and elastic modulus. However, high hardness values are found only in coatings with small nano--grain sizes [8–12].

In Ref. [8], we reported that deposition of Ti–Al–N coatings on to thick Ni–Cr–B–Si–Fe one resulted in improved physical-mechanical properties. In this case, hardness values reach only 22 ± 1.8 GPa, which, first of all, is related to the large nanograin sizes of $17 \div 22$ nm to $34 \div 90$ nm. A thin film with thickness less than 3.5 μm

* corresponding author; e-mail: alexp@i.ua and apogrebnjak@simp.sumy.ua

was deposited onto Ni–Cr–B–Si–Fe thick coating of 60 to 70 μm using magnetron sputtering with the alloyed $Ti_{40}Al_{60}$ target.

In Ref. [9], steel samples were coated with 2.5 μm coating by usage of vacuum-arc source in HF discharge. Fabricated coatings demonstrated high hardness reaching 35 ± 2.1 GPa combined with high wear resistance, scuffing resistance, and low friction coefficient in comparison with standard TiN.

In this paper we discuss the fabrication of multilayered nanocomposite Ti–Al–N/Ti–N/Al_2O_3 coatings, which were prepared using several technologies, which, on our opinion, and on the basis of many previous publications, demonstrate high physical-mechanical characteristics, corrosion properties and high resistance to oxidation under high temperature conditions.

The goal of this work is the fabrication of multi--component combined coatings based on Ti–Al–N/Ti–N/Al_2O_3 on a steel substrate and studies of their structural and physical-mechanical properties.

2. Experimental

Samples of stainless steel 321 of $2.5 \div 3$ mm thickness were coated using plasma-detonation method by the device "Impule-6". The coating, with thickness of about 50 μm, was fabricated from α-Al_2O_3 powder with 23 to 56 μm grain size. Coatings were deposited within 20 mm width, for one pass. Gas expenditures and battery capacity were similar to those applied in Ref. [9]. After the surface purification by glow discharge, TiN coating of 1.8 to 2.2 μm thickness was deposited onto Al_2O_3 coatings using 100 A arc current of Ti cathode and leaking-in N/Ar gas mixture.

Using the alloyed cathode TiAl, Ti–Al–N layers of different thickness in the range of $2.2 \div 2.5$ μm were deposited also in N/Ar medium. The resulting thickness of a three-layer multi-component coating reached 53 to 56.5 μm.

To analyze the coating structure, we used following methods: X-ray diffraction (XRD), transmission electron microscopy (TEM) analysis, scanning electron microscopy with microanalysis (SEM with EDS), and the Rutherford backscattering method (RBS) (He ions of 2.29 MeV and protons of 1.001 MeV) for composition analysis. Electron spectroscopy and corrosion tests were performed using a standard cell [13, 14]. Wear resistance tests were performed according to the cylinder--plane scheme. Transversal and angular cross-sections ($7 \div 10^\circ$ angle) were prepared for several samples to analyze depth element distribution over the total multilayered coating. They were used for electron microscopy, microanalysis, point-by-point XRD-analysis, and nanoindentation.

The elemental distribution in the coatings, before and after corrosion treatment, was evaluated by the RBS at the 5.5 MV Tandem Accelerator of the NCSR DEMOKRITOS/Athens using a deuteron beam of 1.5 MeV energy (scattering angle: 170°, solid angle: $2.54 \times 10''^3$ sr). Nuclear reaction analysis using the same accelerator was used for the determination of the N depth distribution on the samples (^{14}N(d, a)^{12}C nuclear reaction, $E_d = 1.350$ MeV, detector angle: 150°, detector solid angle: $2.54 \times 10''^3$ sr) [13].

For the RBS and nuclear reaction analysis (NRA) measurements a C. Evans & Assoc. scattering chamber equipped with a computer controlled precision goniometer and a laser positioning system was utilized. The vacuum in the scattering chamber was constant (*ca.* 2×10^{-7} Torr). The beam current on the target did not exceed 10 nA, while the beam spot size was 1.5 mm × 1.5 mm. The analysis of the NRA and RBS data was performed using the simulation code RUMP [7].

The corrosion resistance of the prepared coatings was investigated using electrochemical techniques. An AUTOLAB Potentio-Galvanostat (ECO CHEMIE, Netherlands) and Princeton Applied Research corrosion testing cell were used for the electrochemical measurements. A saturated calomel electrode used as a reference electrode and a graphite one as an auxiliary electrode for all measurements.

The tests in 0.5 M H_2SO_4 solution were carried out in the potential region -1000 to $+$ 1500 mV at ambient temperature. Five rapid scans (scan rate = 25 mV/s) followed by one slow scan (scan rate = 0.25 mV/s) were performed on each specimen. The rapid scans allow investigations under constant conditions of the material surface and corroding medium, whereas slow scans lead to predictions of the general corrosion behavior of the material. In all cases the sample surface exposed to the corroding medium was 1 cm^2 [13, 14]. The above-mentioned experimental conditions were also applied for the corrosion tests in HCl and NaCl solutions, whereas the scanning region was from -300 to $+1700$ and from -1000 to $+1000$ mV, respectively [13, 14].

3. Results and discussion

Table I presents the calculated results of nanohardness and elastic modulus for every layer of the multilayered system.

TABLE I

The values of hardness and modulus of elasticity, the size of layers sandwich of nanocomposites combined coatings deposited on stainless steel.

Composition of coating (layer)	H [GPa]	E [GPa]	Grain size [nm]	Thickness of layers [μm]
Ti–Al–N	35 ± 1.8	327 ± 13	$10 \div 12$	$2.2 \div 2.5$
Ti–N	22 ± 6	240 ± 16	$20 \div 35$	1.8 ± 0.2
Al_2O_3	$16 \div 20$	194 ± 8	$10^4 \div 10^5$	$48 \div 52$
steel	4.2	46 ± 2.5	$10^5 \div 10^6$	2×10^3

One can see that nanostructured Ti–Al–N featured the highest hardness of 35 ± 1.8 GPa and the highest elastic modulus 327 ± 17 GPa. Evaluations of grain sizes

performed according to Debye–Sherrer method, demonstrated that the grain size in near surface layer was in the range of 10 to 12 nm, at the same time, the second TiN layer demonstrated sizes of 30 to 35 nm and Al_2O_3 coating demonstrated wide variation of values from units of a micron (5% of all grains) and tens of micron (25%) to grains exceeding 100 nm (less than 20%). Thus, the third layer of Al_2O_3 ceramics turned out to be dispersion--hardened rather than nanostructured one.

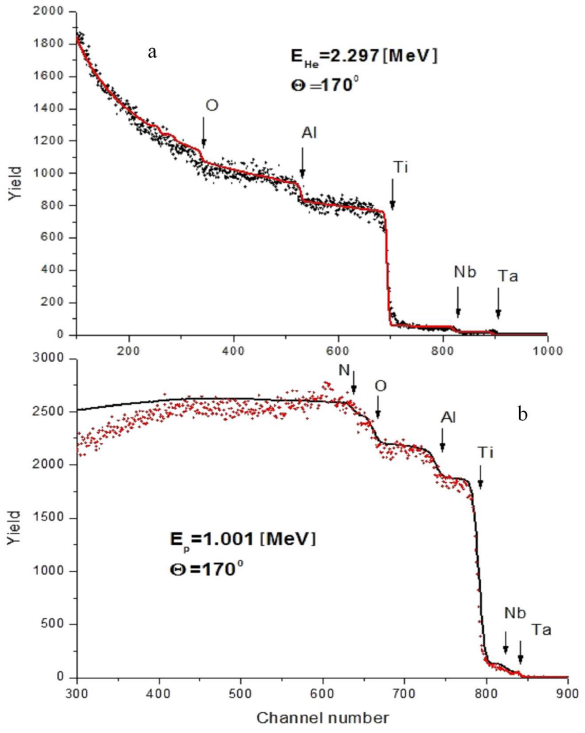

Fig. 1. RBS experimental spectra obtained for multilayered Ti–Al–N/Ti–N/Al_2O_3 coating. Helium ion energy was 2.297 MeV (a) and proton energy was 1.01 MeV (b).

Figure 1 shows RBS spectra of He ions (a) and protons (b). In this coating, Ni, O, Al, Ti elements and small concentration of Nb atoms, as well as very small amount of Ta were observed. The latter came from chamber walls as non-controlled impurity. When the spectrum formed a step, the compound stoichiometry, which was obtained from RBS spectra according to formulae [10, 12] demonstrated $Ti_{60}Al_{40}$ values.

The used proton beam energy was sufficient to analyze the second layer of TiN over its depth and the next one of Al_2O_3 including the interface of Al_2O_3 layer (relative to a substrate). The analyzing proton beam could not reach the back Al_2O_3 interface because of insufficient energy. The images of coating cross-sections showed three layers of different thickness. A visual analysis indicated good quality of the resulting coatings without any pores but with surface roughness following from the plasma-detonation treatment. All subsequent layers repeated this roughness, diminishing it a little degree due to smoothed interfaces between protuberances and valleys. However, after deposition of the thick Al_2O_3, we specially polished surfaces for RBS measurements. The cross-sections were prepared for microanalysis and nanoindentation tests. Point-by-point microanalysis, which was performed in angular cross-section starting from the substrate, demonstrated that the first layer was composed of Ti–Al–N, the second one — of TiN, and the third one of Al_2O_3.

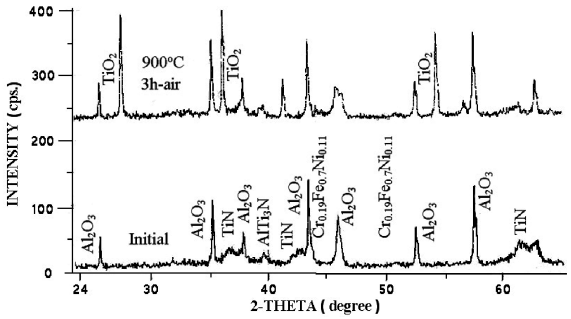

Fig. 2. The diffraction patterns for multilayered nanocomposite Ti–Al–Ni/Ti–N/Al_2O_3 coating after deposition (in several weeks) and after 900 °C annealing in air during 3 h.

Figure 2 shows the diffraction patterns for multilayered nanocomposite coatings of Ti–Al–N/Ti–N/Al_2O_3 at the initial state. As it is seen in this figure, Al_2O_3, TiN, $AlTi_3N$, (AlTi)N phases are presented in this coating. Cr 0.19 Fe 0.7 Ni 0.11 phase, which came from the substrate, was also possible. After 600 °C annealing, the coating phase composition was changed. However, 900 °C annealing during 3 h in air (the diffraction pattern in Fig. 2, the upper curve) resulted in formation of TiO_2 and phase of Al_2O_3 became more microcrystalline and contained only α-Al_2O_3, i.e. total oxidation of Ti and Al occurred as a result of 900 °C annealing in air. Coating hardness also decreased and was equal to 8.8 to 12 GPa. In such a way, the upper two layers were oxidized (probably, the first one — totally and the second one — partially). The layer, which was composed of Al_2O_3, did not demonstrate transition from γ-phase to α-one, possibly because it starts at temperatures higher than 900 °C.

Auger-electron microscopy, which was performed for these coatings, demonstrated Ti, N, Al, O, and C elements. At initial moment of deposition, concentration of these elements was changed, but after the etching during more than 12 min, their profile did not change. Additional studies performed using nuclear reactions method, allowed us to obtain depth element profiles for two upper layers including the interface between second and third layers. Thickness of Ti–Al–N and Ti–N layers was accurately measured. It amounts to 4.27 μm. Measurements after 900 °C annealing of the multilayer demonstrated essential changes of element concentration profiles over depth. The upper layer was enriched with oxygen and

carbon, which indicated formation of Ti and Al oxides. This was confirmed by XRD analysis.

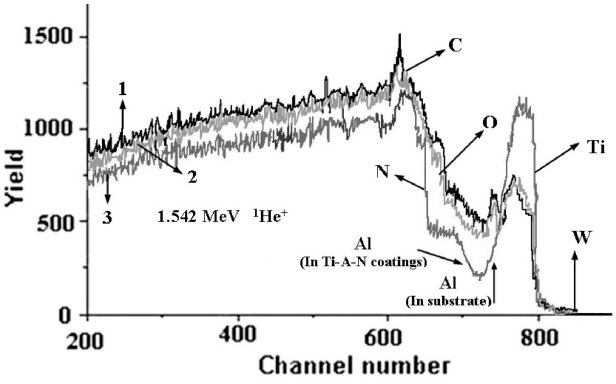

Fig. 3. Hydrogen RBS spectra obtained for multilayered Ti–Al–N/Ti–N/Al_2O_3 coating for various conditions:.curve 1 — initial state Ti–Al–N/Ti–N/Al_2O_3; curve 2 — after high-current electron beam treatment with 10 J cm^{-2}: curve 3 — after 900 °C annealing in air during 3 h.

Figure 3 shows RBS results for all basic elements of the coating before and after annealing. Obtained results demonstrated essential changes, which occurred in the coating: Ti concentration (peak) decreased, Ti profile was smoothed, TiO_2 compound was formed, N concentration decreased, Al was redistributed, its state was changed, i.e. a part of Al formed Al_2O_3 oxide. This agreed well with XRD results before and after annealing in air under 900 °C during 3 h (Fig. 2).

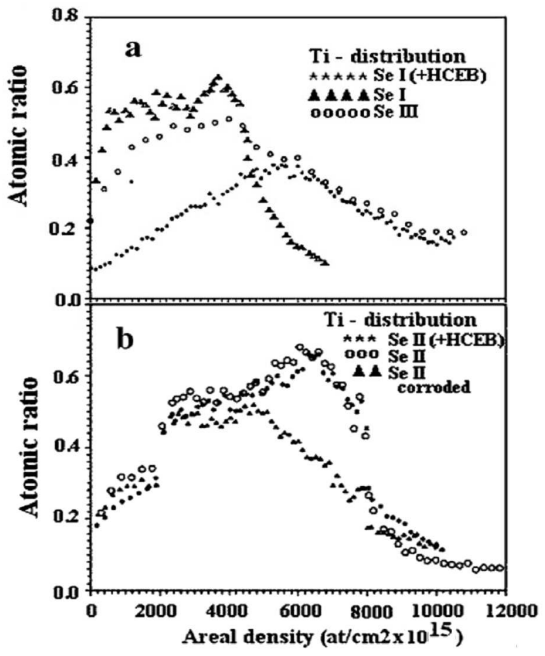

Fig. 4. (a) and (b) Ti distribution obtained from the RBS simulated spectra.

Figures 4a and b present the Ti-distribution in several coated samples obtained by RBS. The high-current electron beams (HCEB) treatment in case of series I samples leads to the significant inward shift of the Ti-distribution and to decrease of the Ti-content in the layers close to surface (see Fig. 6a). Chromium and aluminum were observed at the depth of *ca.* 1.0 and 2.2 mm in case of series I samples not processed and processed under HCEB treatment, respectively, according to the simulation results. In case of series III samples (without a Cr interlayer) the titanium diffusion is more intense. On the other hand, only limited titanium diffusion was observed in case of series II samples, where the TiN and Cr-layers are thicker (Fig. 4b). In this case aluminum and chromium were observed at the depth of *ca.* 1.6 and 2.4 mm for the untreated and HCEB treated samples, respectively.

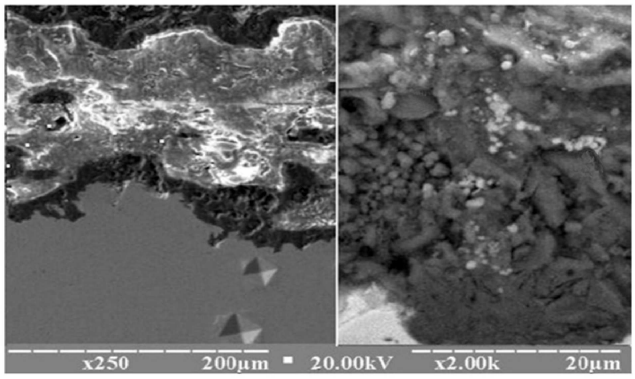

Fig. 5. Structure of transversal cross-section in multilayered nano–microcomposite coating (left) and surface image (right) in the initial state after deposition (in three months).

Figures 5a, b show images for coating surfaces before and after annealing in air at 600 °C, and for etched angular cross-sections. These images demonstrated no essential changes in coating structure and element composition. One can see a distinct boundary of the coating deposited using vacuum-arc source, namely (Ti–N), Ti–Al–N layer with a thick Al_2O_3 coating fabricated using plasma-detonation technology. Point-by-point microanalysis performed at several points of the coating surface and across the cross-section did not reveal essential changes in its element composition except increased C and O concentrations, and a little lower N concentration. Thereby, thermal annealing of three-layered nanocomposite coating even in air till 600 °C temperature did not affect element and structure composition of coatings, which was not the case for electron beam annealing (till melting).

Measurements of lattice parameters for TiN, (Ti,Al)N, and Al_2O_3 coatings demonstrated that 600 °C annealing decreased stresses arising in lattices: both macrostresses at film–film and film–thick coating interfaces and microstresses arising in nano- and micrograin structures.

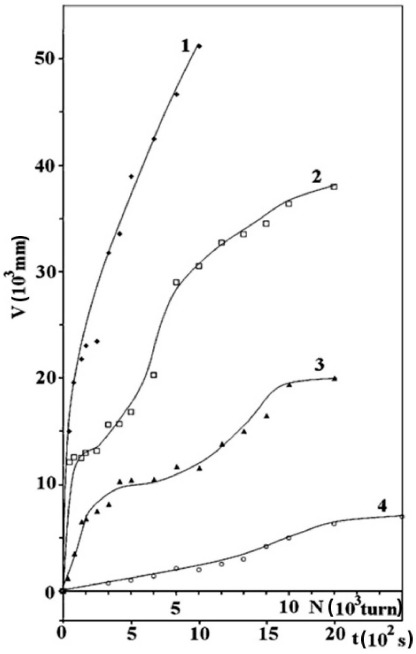

Fig. 6. Dependences of material wear tested by cylinder friction over the sample surfaces: 1 — the initial state; 2 — the Al_2O_3 coating; 3 — TiN/Al_2O_3 coating; 4 — multilayered nano–microcomposite coating of Al–N/Ti–N/Al_2O_3.

Figure 6 shows results of wear tests, which were performed according to the plane-cylinder scheme. These results demonstrate that the most essential wear occurred in the substrate surface (curve 1). After deposition of Al_2O_3 coating by plasma-detonation technology (curve 2) wear sharply decreased. In the case of TiN deposition, wear was lower than in the case of Al_2O_3 (curve 3). The lowest wear was found in the case of multilayered coating Ti–Al–N/Ti–N/Al_2O_3 (curve 4) [9, 12].

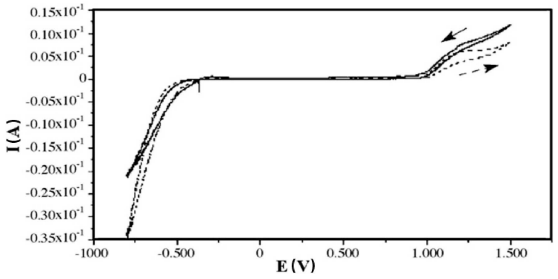

Fig. 7. Potentiodynamic polarization curves of series I samples slow scan 0.17 mV/s (a) without (-) and (b) with (---) HCEB treatment.

Figures 7 and 8 show some characteristic potentiodynamic polarization curves of the coated samples after treatment in 0.5 M H_2SO_4 solution at ambient temperature, whereas the corresponding corrosion data are listed in Table II. The corrosion potential (E_{corr}) in case of uncoated steel sample was found to be −445 mV whereas a significant decrease was observed in case of coated samples. The decrease of E_{corr} and corrosion and passivation current density in case of coated steel samples indicates the enhancement of their corrosion resistance due to protective action of the deposited layer.

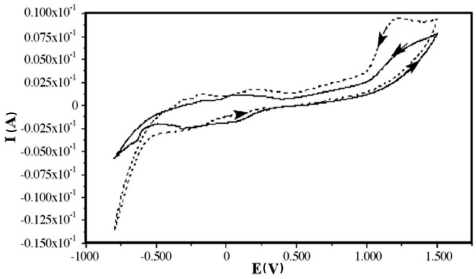

Fig. 8. Potentiodynamic polarization curves of series II samples (rapid scan) (a) without (-) and (b) with HCEB treatment.

TABLE II

Corresponding corrosion data samples after treatment in 0.5 M H_2SO_4.

Sample	E_{corr} [mV]	i_{corr} [mA]	i_{corr} [mA]	E_{pas} [mV]	E_{rep} [mV]
Series I: Al_2O_3+Cr (0.1–0.2 μm) + TiN (0.5–1.2 μm)	−214	2.2	1.0	979	1022
Series II: Al_2O_3+Cr (2–3 μm) + TiN (0.5–1.2 μm)	−330	0.62	1.2	986	1022
Series III: Al_2O_3+Cr (0.1–0.2 μm) + TiN (0.5–1.2 μm)	−273	1.1	0.7	979	11014

Enhanced corrosion resistance was observed in cases of series I and II samples due to quality of triple coating and presence of Cr-layer improving the adhesion of the coating to the substrate. This was mainly observed during the slow scan rate measurements. The improvement was higher in case of series II samples subjected to HCEB treatment, due to inward diffusion of the titanium nitride layer and the increased thickness of the coating. The good quality of coating in cases I and II was also confirmed by other techniques (RBS, SEM). The series III samples without HCEB treatment and those of series IV exhibited poor adhesion, most probably due to lack of the Cr-interlayer, and were finally destroyed during the testing (slow scan rate measurement).

Corrosion tests performed in Electro-Chemical Lab (Thessaloniki, Greece) using international standards in 0.5 M H_2SO_4 solution and by simple microweighing after definite time period (3 to 6 months) in NaCl and HCl solutions, demonstrated high coating resistance in comparison with that of stainless steel 321 substrate (European standards).

4. Conclusion

The fabricated multilayered nano–microcomposite coatings based on Ti–Al–N–Ti–N/Al_2O_3 system featured thermal stability in air till 900 ℃. They also featured high wear resistance under cylinder friction over their surfaces and high corrosion resistance in NaCl and H_2SO_4 medium. However, 900 ℃ annealing resulted in total oxidation of the upper Ti–Al–N layer and partial oxidation of Ti–N one. The coating hardness decreased more than by factor of 2. At the same time, electron pulsed beam (without melting) did not decrease surface hardness, possibly, due to its short-time action. However, it results in redistribution of impurities (coating components) at interfaces of this multilayered coating.

Acknowledgments

The work was fulfilled within the frameworks of ISTCs K-1198 project and partially within the project for NAS of Ukraine "Nano-Systems, Nano-Composites, and Nano-Materials".

The authors are thankful to colleagues Yu.A. Kravchenko, A.D. Mikhailov, and V.S. Kshnyakin from Sumy Institute for Surface Modification, Dr. S. Kislitsyn from Institute of Nuclear Physics of National Nuclear Center of Kazakhstan for their help in experiments, as well as Dr. F. Noly, Prof. P. Misaelides from Thessaloniki, Greece for their corrosion tests.

The work was funded by the project NAS Ukraine and ISTC K-1198.

References

[1] J. Musil, H. Hruby, *Thin Solid Films* **365**, 104 (2000).

[2] V.P. Sergeev, M.V. Fedorischeva, A.V. Voronov, O.V. Sergeev, V.P. Yanovski, S.G. Psakhie, *Proc. Tomsk Polytechnic University* **309**, 149 (2006).

[3] N.V. Prodanov, A.V. Khomenko, *Surf. Sci.* **604**, 730 (2010).

[4] N.V. Prodanov, A.V. Khomenko, *J. Phys. Chem.* **114**, 19958 (2010).

[5] J. Zhu, L. Ye, F. Li Wang, *Appl. Mech. Mater.* **44-47**, 2504 (2011).

[6] P. Budzynski, J. Sielanko, Z. Surowiec, P. Tarkowski, *Vacuum* **83**, S186 (2009).

[7] L.R. Doolittle, *Nucl. Instrum. Methods Phys. Res. B* **15**, 227 (1986).

[8] A.D. Pogrebnjak, A.A. Drobyshevskaia, V.M. Beresnev, M.K. Kylyshkanov, G.V. Kirik, S.N. Dub, F.F. Komarov, A.P. Shypylenko, Yu.Xh. Tuleushev, *J. Tech. Fiz.* **81**, 124 (2011).

[9] V.M. Beresenev, A.D. Pogrebnyak, P.V. Turbin, S.N. Dub, G.V. Kirik, M.K. Kylyshkanov, O.M. Shvets, V.I. Gritsenko, A.P. Shypylenko, *J. Friction Wear* **31**, 349 (2010).

[10] A.D. Pogrebnjak, Yu.A. Kravchenko, S.B. Kislitsyn, Sh.M. Ruzimov, F. Noli, P. Misaelides, A. Hatzidimitriou, *Surf. Coat. Tech.* **201**, 2621 (2006).

[11] A.D. Pogrebnjak, M.M. Danilenok, A.A. Drobyshevskaia, V.M. Beresnev, N.K. Erdybaeva, G.V. Kirik, S.N. Dub, V.S. Rusakov, V.V. Uglov, A.P. Shipilenko, Yu.Zh. Tuleushev, *Russ. Phys. J.* **52**, 1317 (2009).

[12] N.A. Azarenkov, V.M. Beresnev, A.D. Pogrebnjak. *Structure and Properties of Protective Coatings and Modified Layers*, KhNU, Kharkov 2007, p. 560.

[13] P. Misaelides, A. Hatridimitriou, F. Noli, A.D. Pogrebnjak, Y.N. Tyurin, S. Kosionidis, *Surf. Coat. Technol.* **290**, 180 (2004).

[14] *Laboratory Corrosion Tests and Standards*, Eds. G.S. Haynes, R. Baboian, ASTM, Philadelphia 1985.